

Perturbations induced by a molecular cloud on the young stellar disc in the Galactic Centre

Michela Mapelli^{1*}, Alessia Gualandris² and Tristen Hayfield³

¹*INAF-Osservatorio Astronomico di Padova, Vicolo dell'Osservatorio 5, I-35122, Padova, Italy*

²*Department of Physics and Astronomy, University of Leicester, Leicester, LE1 7RH, United Kingdom*

³*Max Planck Institute for Astronomy, Königstuhl 17, D-69117 Heidelberg, Germany*

ABSTRACT

The Galactic centre (GC) is a crowded environment: observations have revealed the presence of (molecular, atomic and ionized) gas, of a cusp of late-type stars, and of ~ 100 early-type stars, about half of which lying in one or possibly two discs. In this paper, we study the perturbations exerted on a thin stellar disc (with outer radius ~ 0.4 pc) by a molecular cloud that falls towards the GC and is disrupted by the supermassive black hole (SMBH). The initial conditions for the stellar disc were drawn from the results of previous simulations of molecular cloud infall and disruption in the SMBH potential. We find that most of the gas from the disrupted molecular cloud settles into a dense and irregular disc surrounding the SMBH. If the gas disc and the stellar disc are slightly misaligned ($\sim 5 - 20^\circ$), the precession of the stellar orbits induced by the gas disc significantly increases the inclinations of the stellar orbits (by a factor of $\sim 3 - 5$ in 1.5 Myr) with respect to the normal vector to the disc. Furthermore, the distribution of orbit inclinations becomes significantly broader. These results might be the clue to explain the broad distribution of observed inclinations of the early-type stars with respect to the normal vector of the main disc. We discuss the implications for the possibility that fresh gas was accreted by the GC after the formation of the disc(s) of early-type stars.

Key words: methods: numerical – stars: kinematics and dynamics – Galaxy: centre – black hole physics – ISM: clouds

1 INTRODUCTION

The compact radio source Sgr A*, located at the very centre of our Galaxy, coincides with a high concentration of mass ($\approx 4 \times 10^6 M_\odot$), almost certainly a supermassive black hole (SMBH, Genzel et al. 2003; Schödel et al. 2003; Ghez et al. 2003, 2005). More than a hundred young massive stars have been observed in the vicinity of Sgr A* (Krabbe et al. 1991; Morris 1993; Krabbe et al. 1995; Genzel et al. 2003). Many of them are O-type and Wolf-Rayet (WR) stars. About half of the early-type stars lie in a thin disc with radius $0.04 \text{ pc} \lesssim r \lesssim 0.5 \text{ pc}$ and average eccentricity $e \sim 0.3 - 0.4$ (Bartko et al. 2009; Lu et al. 2009; Yelda et al. 2012; Do et al. 2013; Lu et al. 2013). This disc is called clock-wise (CW) disc, because it shows CW motion when projected on the plane of the sky (Genzel et al. 2003; Paumard et al. 2006). The CW disc is likely warped, as the orientation of its normal vector changes by several degrees ($\sim 60^\circ$, according to Bartko et al. 2009) from its inner to its outer edge. A frac-

tion of the remaining early-type stars show counterclockwise motion, which may indicate the presence of a second dissolving disc (Lu et al. 2006, 2009; Bartko et al. 2009). The age of the observed early-type stars is $t_{\text{age}} \approx 2.5 - 6$ Myr (Lu et al. 2013; see Paumard et al. 2006 for a previous estimate $t_{\text{age}} = 6 \pm 2$ Myr). Furthermore, Yusef-Zadeh et al. (2013) found indications of gas outflows, suggesting recent star formation (10^{4-5} yr) within 0.6 pc of SgrA*. The ~ 20 stars closest to SgrA* ($\lesssim 0.04 \text{ pc} \sim 1 \text{ arcsec}$) are B stars, with an age 20–100 Myr. These, named the S-stars, have very eccentric and randomly oriented orbits (Schödel et al. 2003; Ghez et al. 2003, 2005; Eisenhauer et al. 2005; Gillessen et al. 2009). The ensemble of the (both young and old) stars in the central few parsecs is often referred to as the nuclear star cluster (NSC) of the Milky Way (MW).

The Galactic centre (GC) is a very crowded environment not only for the stellar population, but also for the gas. A molecular torus, the circumnuclear ring (CNR, Genzel et al. 1985; Güsten et al. 1987; Yusef-Zadeh et al. 2004; Christopher et al. 2009; Oka et al. 2011), is located at ~ 2 pc from SgrA*, and is on the verge of forming stars

* E-mail: michela.mapelli@oapd.inaf.it

(Yusef-Zadeh et al. 2008). Furthermore, the innermost 3 pc of the GC are extremely rich in ionized gas (e.g., Zhao et al. 2009, and references therein). Finally, two molecular clouds (the M-0.02-0.07 and the M-0.13-0.08 cloud, Solomon et al. 1972; Novak et al. 2000) lie within 20 pc of the GC.

The origin of the early-type stars is puzzling, as the strong tidal field exerted by the SMBH is expected to disrupt any molecular cloud before it reaches the distance of the CW disc. On the other hand, a disrupted molecular cloud might spiral towards the SMBH and form a gas disc around it, sufficiently dense to fragment into stars (Levin & Beloborodov 2003; Goodman 2003; Goodman & Tan 2004; Milosavljevic & Loeb 2004; Nayakshin & Cuadra 2005; Rice et al. 2005; Alexander et al. 2008; Collin & Zahn 2008; Bonnell & Rice 2008; Mapelli et al. 2008; Wardle & Yusef-Zadeh 2008; Hobbs & Nayakshin 2009; Alig et al. 2011; Jiang & Goodman 2011; Namekata & Habe 2011; Mapelli et al. 2012, hereafter M12; Lucas et al. 2013; Alig et al. 2013). In particular, M12 simulated the infall of a molecular cloud towards the GC. In the M12 simulations, the molecular cloud is disrupted by the SMBH tidal shear, and settles into a dense gas disc, which fragments into self-gravitating clumps. These clumps, or proto-stars, lie in a disc at a distance of 0.1–0.4 pc with moderately eccentric orbits ($e \sim 0.2 - 0.4$). The properties of the stellar disc reproduce quite well the observations of the CW disc, but cannot explain the counterclockwise stars as well as the S-stars. On the other hand, M12 integrates the evolution of the cloud only for ~ 0.5 Myr, while the early-type stars are $\sim 2.5 - 6$ Myr old (Lu et al. 2013).

The GC is such a crowded environment that many external forces might have influenced the orbital evolution of the CW disc after its formation. First, the stellar cusp of late-type stars induces precession on the orbits of a stellar disc (e.g. Löckmann et al. 2009). This is expected to significantly affect the eccentricity distribution (Madigan et al. 2009; Gualandris et al. 2012, hereafter G12). Furthermore, a massive perturber, such as an intermediate-mass black hole (Gualandris & Merritt 2009; Gualandris et al. 2010; Perets & Gualandris 2010), the CNR (Haas et al. 2011a; Haas et al. 2011b), a second stellar disc (Löckmann et al. 2008; Löckmann & Baumgardt 2009; Löckmann et al. 2009), or a second molecular cloud infalling towards SgrA* is expected to induce a precession on the CW disc, and it may also excite the Kozai resonance (Kozai 1962; Lidov 1962). In this paper, we simulate the infall of a second molecular cloud toward the SMBH, and we study the influence that the second cloud has on the orbits of a pre-existing stellar disc. As initial conditions for the pre-existing stellar disc, we adopt the outcomes of run E in M12.

2 N-BODY SIMULATIONS

For our simulations, we used the N-body/smoothed particle hydrodynamics (SPH) code GASOLINE (Wadsley et al. 2004), upgraded with the Read et al. (2010) optimized SPH (OSPH) modifications, to address the SPH limitations outlined, most recently, by Agertz et al. (2007).

Table 1 shows a summary of the runs that will be pre-

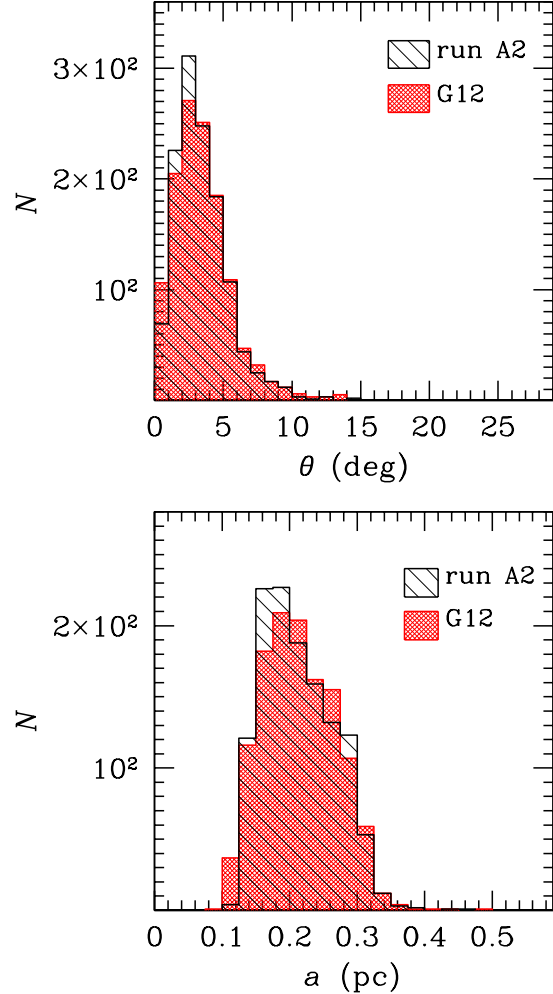


Figure 1. Top (bottom): distribution of inclinations (semi-major axes) at $t = 1.5$ Myr. The inclinations are measured by the angle θ , between the normal vector to the orbit of a single star and the total angular momentum vector of the stellar disc (see Appendix A). Cross-hatched red histogram: simulation from G12. Hatched black histogram: run A2.

sented in this paper. In all the runs, we simulate a disc of 1252 star particles orbiting the SMBH. The SMBH is represented by a sink particle, with initial mass $M_{\text{SMBH}} = 3.5 \times 10^6 M_{\odot}$ (Ghez et al. 2003), sink radius $r_{\text{acc}} = 5 \times 10^{-3}$ pc and softening radius $\epsilon = 1 \times 10^{-3}$ pc.

The disc of star particles is obtained from run E of M12, with the same procedure as described in G12. In particular, we assume that each self-bound clump formed in run E of M12 becomes a star, without accreting any further gas particles after $t = 4.8 \times 10^5 \text{ yr}^1$. Thus, we replace each gas particle with a single star particle having mass equal to the total mass of the gas clump, position and velocity corresponding to those of the centre-of-mass of the clump. The resulting simulated mass of the disc is $4.1 \times 10^3 M_{\odot}$ (see M12). The best-fitting initial mass function (IMF) is given

¹ This assumption is quite conservative for the mass of stars, as it is realistic to expect further gas accretion in run E of M12.

Table 1. Initial conditions.

Run	Stellar Cusp ^a	Perturber ^b	α ($^\circ$) ^c
A1	No	No	–
A2	Yes	No	–
B1	No	Yes	0
B2	Yes	Yes	0

^a The stellar cusp is the rigid potential corresponding to the density distribution in Schödel et al. (2007). ^b The perturber is a MC falling towards the GC. ^c α is the inclination between the initial orbit of the MC (when present in the simulation) and the plane of the stellar disc. $\alpha = 0$ means that the orbit of the cloud lies in the plane of the stellar disc.

by a single power law with index $\alpha = 1.50 \pm 0.06$ (see M12 for details), consistent with Lu et al. (2013, $\alpha = 1.7 \pm 0.2$). Considering that M12 simulations cannot resolve stellar masses $< 1.3 M_\odot$, this corresponds to an expected total mass of the disc $\approx 4.5 \times 10^3 M_\odot$ (assuming $\alpha = 1.50$). This value is consistent with most observations (e.g. Paumard et al. 2006; Bartko et al. 2009), but is a factor of ~ 3 lower than the most recent results (Lu et al. 2013). Finally, the stellar disc has average semi-major axis $\langle a \rangle = 0.21 \pm 0.04$ pc, average inclination² $\langle \theta \rangle = 2.4 \pm 1.5^\circ$, and average eccentricity $\langle e \rangle = 0.29 \pm 0.04$.

The high density and the clumpiness of the gas disc at $t = 4.8 \times 10^5$ yr in run E of M12 make prohibitive to continue the simulation as it is. Thus, in our initial conditions, we instantaneously removed the gas left in the first disc, to prevent our simulations from stalling before the infall of the second cloud. For the issues related to this assumption, see the discussion in Section 3.4.

In runs A2 and B2, we also add a rigid potential, to account for the stellar cusp surrounding Sgr A*. The overall density profile of the stellar cusp goes as $\rho(r) = 2.8 \times 10^6 M_\odot \text{pc}^{-3} (r/0.22 \text{pc})^{-\gamma}$, where $\gamma = 1.2$ (1.75) for $r < 0.22$ pc ($r > 0.22$ pc), consistent with the values reported in Schödel et al. (2007). Runs A2 and B2 will be referred to as runs ‘with cusp’, while runs A1 and B1 will be dubbed runs ‘without cusp’.

In runs B1 and B2, we simulate the infall of a second molecular cloud towards the GC, to study the perturbations induced by the cloud on the orbits of the stellar disc. In runs A1 and A2, we do not include the second molecular cloud: the stellar disc evolves under the influence of the SMBH, and, in the case of run A2, also under the influence of the rigid stellar cusp. Runs A1 and A2 were performed just for comparison with the other two runs.

The perturber cloud is simulated as in M12. In particular, it is a spherical cloud with a radius of 15 pc and a mass of $1.3 \times 10^5 M_\odot$. The cloud is seeded with supersonic turbulent velocities and marginally self-bound (see Hayfield et al. 2011). The centre-of-mass of the cloud is initially at 25 pc from the SMBH. The orbit of the cloud was chosen so that the impact parameter with respect to the SMBH is 10^{-2} pc and the initial velocity is one tenth of the escape velocity from the SMBH at the initial distance (i.e. the orbit is bound and highly eccentric). The orbit of the cloud lies

in the plane of the stellar disc ($\alpha = 0$, see Table 1). As in run E of M12, we include radiative cooling in all our simulations. The radiative cooling algorithm is the same as that described in Boley (2009) and in Boley et al. (2010). D’Alessio et al. (2001) opacities are used, with a $1 \mu\text{m}$ maximum grain size. The irradiation temperature is $T_{\text{irr}} = 100$ K everywhere. The mass of the gas particles in each simulation is $0.4 M_\odot$ and the softening length 10^{-3} pc. Given the low mass resolution, these simulations cannot be used to study gas fragmentation. In a forthcoming paper, we will show new high-resolution runs focused on this aspect, while in the current paper we are interested in the role of the cloud as perturber of the pre-existing stellar disc.

The code used for our simulations adopts a kick-drift-kick leapfrog integrator. This scheme is known to be rather inaccurate in the short-term integration of the orbits, while it preserves well energy and angular momentum on the long term evolution (e.g., Zemp et al. 2007; Dehnen & Read 2011). This may damp any secular changes in eccentricity (e.g., Zemp et al. 2007). On the other hand, the adopted code is the best compromise between describing the orbits accurately and following the thermodynamical and dynamical evolution of a living cloud (rather than assuming a rigid potential for the gas, as done in previous work).

We checked the limits of our numerical approach by comparing them with the results of G12, who used a Hermite integration scheme (implemented in the direct-summation N-body code ϕ GRAPE, Harfst et al. 2007). In Fig. 1, the distribution of semi-major axes and inclinations obtained at $t = 1.5$ Myr by G12 are compared with the same distributions derived at $t = 1.5$ Myr for our run A2 (whose main ingredients are the same as in G12). No evident differences appear between G12 and our run A2, by looking at Fig. 1. The Kolmogorov-Smirnov test indicates a 80 (30) per cent probability that the distribution of semi-major axes (inclinations) is the same in G12 and in run A2. Such probabilities are quite high, considering the intrinsic differences of the two runs. Other checks (e.g. reducing the time stepping, changing the number of neighbours, substituting the SMBH particle with a rigid potential, integrating some analytic orbits) demonstrated that our results are robust and fairly describe the effects of precession on the stellar orbits. Furthermore, stochastic fluctuations (between different realizations of run A2) change the orbital parameter distributions by less than ~ 10 per cent (i.e. do not significantly affect the mean values of the orbital parameters).

The simulations presented in this paper ran on the Fermi IBM Blue Gene/Q at CINECA (through CINECA Award N. HP10CL51UF, 2012). Runs B1 and B2 required approximately 100k CPU hours each.

3 RESULTS

3.1 The disruption of the cloud and the formation of the gas disc

In our runs B1 and B2, the second molecular cloud spirals towards the GC, and is quickly disrupted by the tidal force exerted by the SMBH. The disruption of the cloud starts at $t \approx 10^5$ yr since the beginning of the simulations, i.e. $\approx 6 \times 10^5$ yr after the infall of the first cloud (simulated in

² For the definition of the coordinate system, see Appendix A.

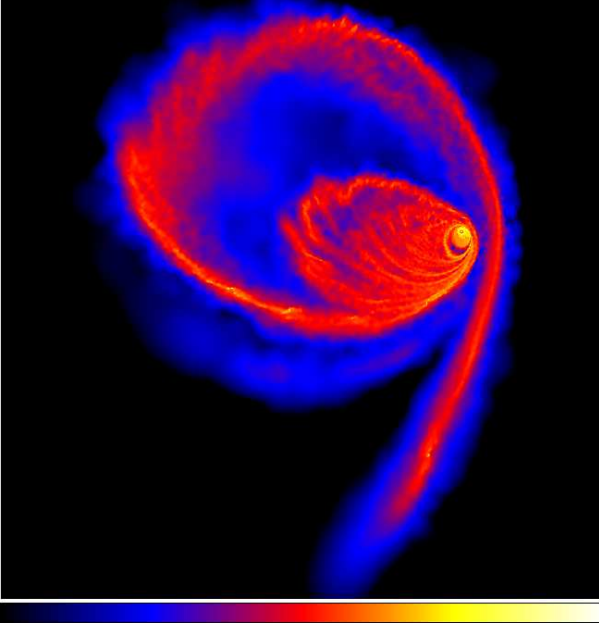


Figure 2. Projected density of gas in run B1 at $t = 1.5$ Myr. The gas disc is seen face-on. The box measures 35 pc per edge. The color map is logarithmic, ranging from 2×10^{-4} to $2 \times 10^8 M_{\odot} \text{pc}^{-3}$.

M12). At $t \approx 3 - 5 \times 10^5$ yr since the beginning of the simulation, a dense gaseous ring forms, surrounding the SMBH. In the next Myr, the ring is fueled by fresh gas coming from the remnant of the disrupted molecular cloud (see Fig. 2). For this reason, the central gas disc looks more like a series of streamers than a coherent thin disc (see Fig. 3). We notice that the gravitational potential exerted on the cloud is slightly different in run B1 and B2, since a spherical stellar cusp is included only in run B2. Thus, the orbits of the streamers are slightly different in the two runs.

The initial inclination of the orbit of the cloud is nearly preserved during the evolution and the tidal disruption. In runs B1 and B2, the orbit of the second molecular cloud is in the plane of the stellar disc ($\alpha = 0$), and the gas disc and the pre-existing stellar disc are nearly coplanar (see Fig. 3).

On the other hand, the gas disc is not a rigid body, but is instead composed of many concentric annuli and streamers, all of which may have slightly different ($\sim 5^\circ$) mutual inclinations (see Figs. 3, 4 and 5). Furthermore, the fact that the cloud is seeded with supersonic turbulence implies that clumps and filaments form in the molecular cloud before disruption. This determines local changes in the geometry of the infalling cloud, and is source of important stochastic fluctuations in the structure of the gas disc, between different simulations. In particular, we remind that the initial radius of the cloud is ~ 15 pc, while the radius of the stellar disc is less than one pc: even small density fluctuations inside the cloud can significantly affect the geometry of the encounter between the stellar disc and the cloud.

In particular, Figs. 4 and 5 show how the gas disc assembles between 0.5 and 1.5 Myr. We notice that the orbits of the streamers can change with time, as long as the disrupted molecular cloud re-fuels the inner disc with fresh gas. This makes the interplay between stellar disc and gas disc(s)

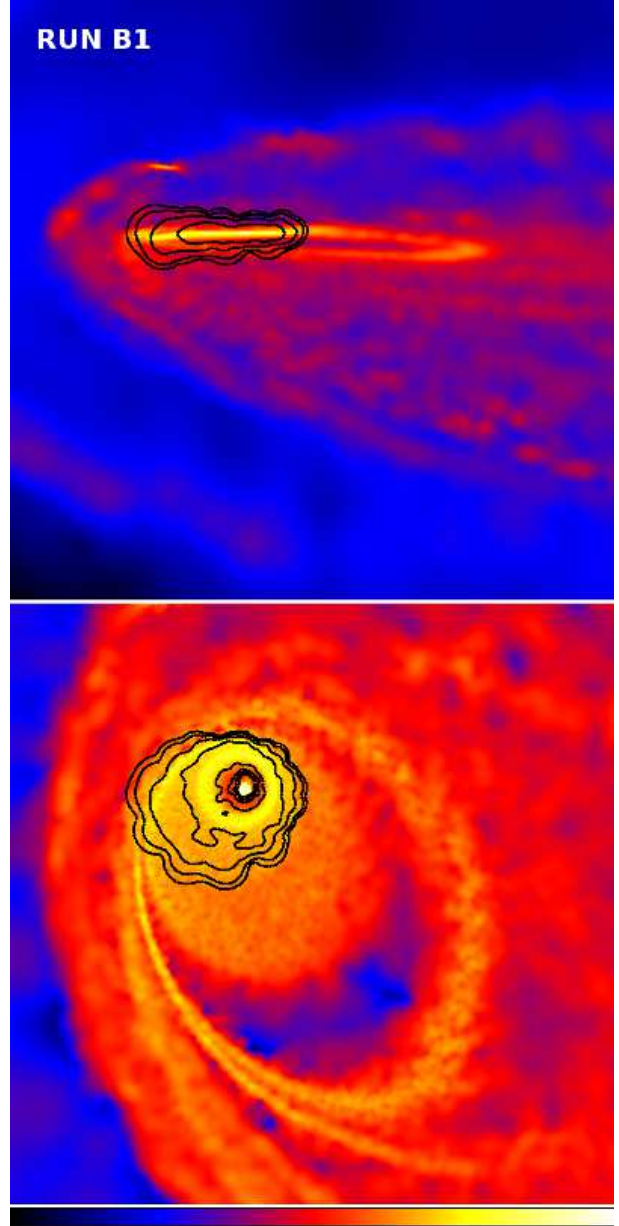


Figure 3. Projected density of gas in run B1 at $t = 1.5$ Myr. The color map is logarithmic, ranging from 2×10^{-4} to $2 \times 10^8 M_{\odot} \text{pc}^{-3}$. The contours show the projected density of stars in the stellar disc. Top panel: the stellar disc is seen edge-on. Bottom-panel: the stellar disc is seen face-on. Each box measures 2.3 pc per edge.

very complicated. It is apparent that while the stars define a thin and coherent disc, the gas is distributed in a series of streamers, with different angular momentum directions.

Finally, by the end of the simulation, when the cloud is entirely disrupted and the gas discs are completely settled (i.e. the shocks and the cooling induced by the disruption are over and almost no new gas is accreted), the situation is even more complex. The bottom panels of Figs. 4 and 5 show the inner 2 pc of run B2 at $t = 1.5$ Myr. It is apparent that there are at least two different gas rings: a inner one, with radius ~ 0.4 pc (similar to the stellar disc), and a outer one, with radius ~ 1.5 pc. While the inner gas disc is almost

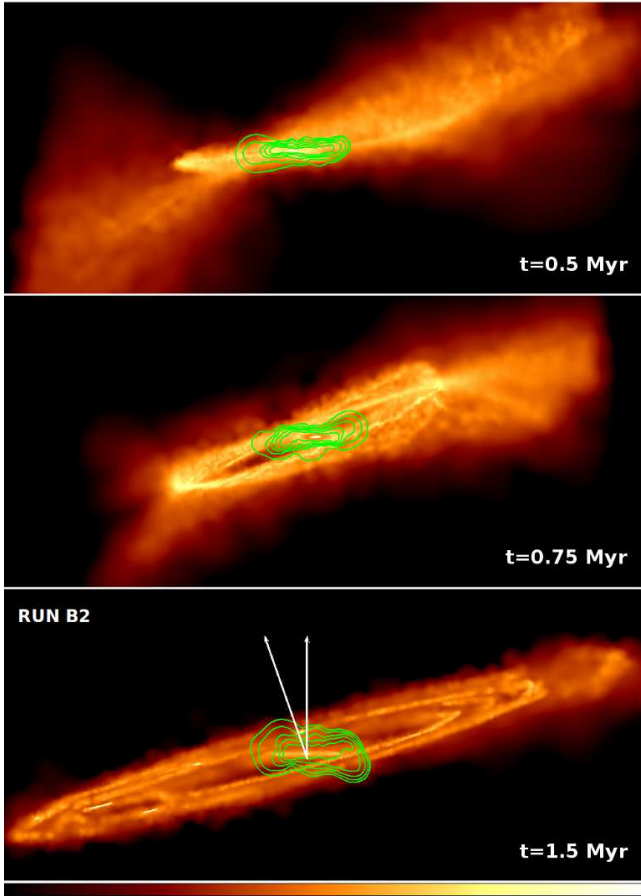


Figure 4. Projected density of gas in run B2 at $t = 0.5$, 0.75 and 1.5 Myr in the top, central and bottom panel, respectively. The color map is logarithmic, ranging from 2×10^{-2} to $2 \times 10^{10} M_{\odot} \text{pc}^{-3}$. The contours show the projected density of stars in the stellar disc. The box size is 4.0×1.8 pc. The projection was chosen so that the total angular momentum of the stellar disc is aligned to the vertical axis of the plot. The two white arrows in the bottom panel show the direction of the total angular momentum of the stellar disc and the total angular momentum of the outer gas disc. The length of the arrows is arbitrary.

coplanar with the stellar disc, the angular momentum vector of the outer gas disc is inclined by $\sim 15-20^{\circ}$ with respect to the angular momentum vector of the stellar disc. The outer gas ring may play the same role as the CNR observed in our Galaxy.

Figs. 6 and 7 show the angular momentum distribution of gas particles moving on bound orbits around the SMBH (with semi-major axis $0.1 \leq a/\text{pc} \leq 10$) in run B1 and B2, respectively. The top and the bottom panel refer to time $t = 0.5$ and 1.5 Myr, respectively. The coordinate system refers to the total angular momentum of the stellar disc at a given time t , as defined in Appendix A. We remind that particles belonging to a razor thin disc aligned with the stellar disc have $\cos \theta = 1$ and can assume any possible value of ϕ . Instead, a razor thin disc that is misaligned with respect to the stellar disc defines an infinitely small circle in the $\cos \theta, \phi$ plane. The larger the opening angle of the disc, the larger the circle it defines in the $\cos \theta, \phi$ plane. The

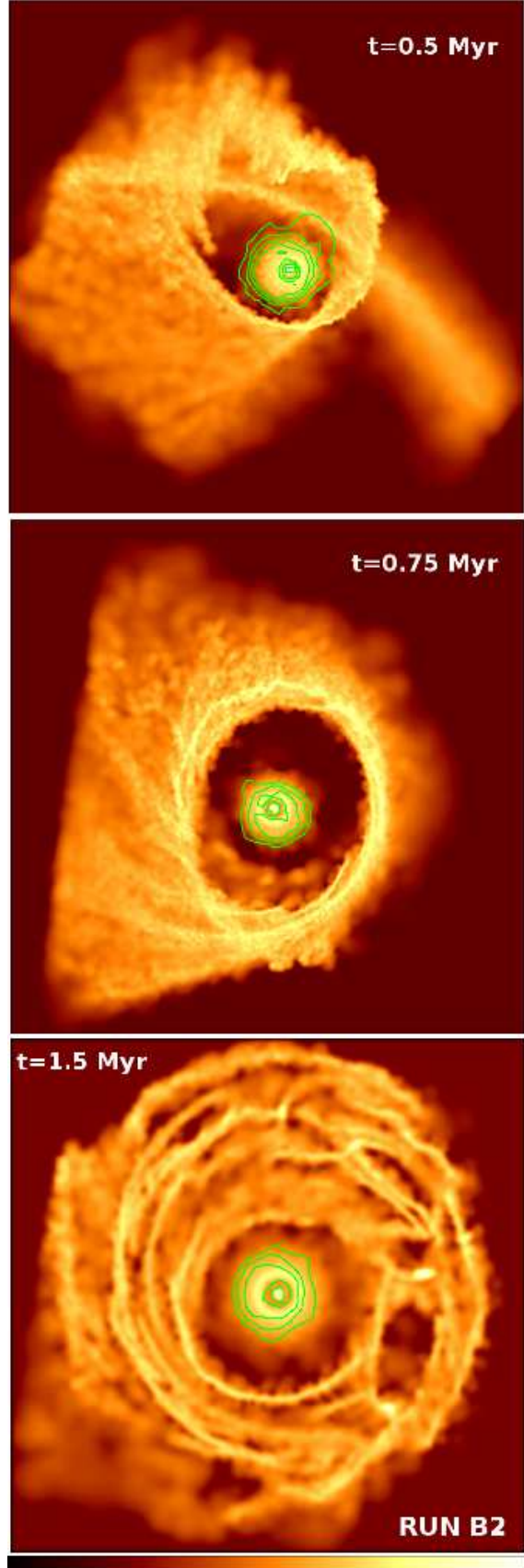


Figure 5. The same as Fig. 4, but rotated so that the stellar disc is seen face on. The box size is 4×4 pc.

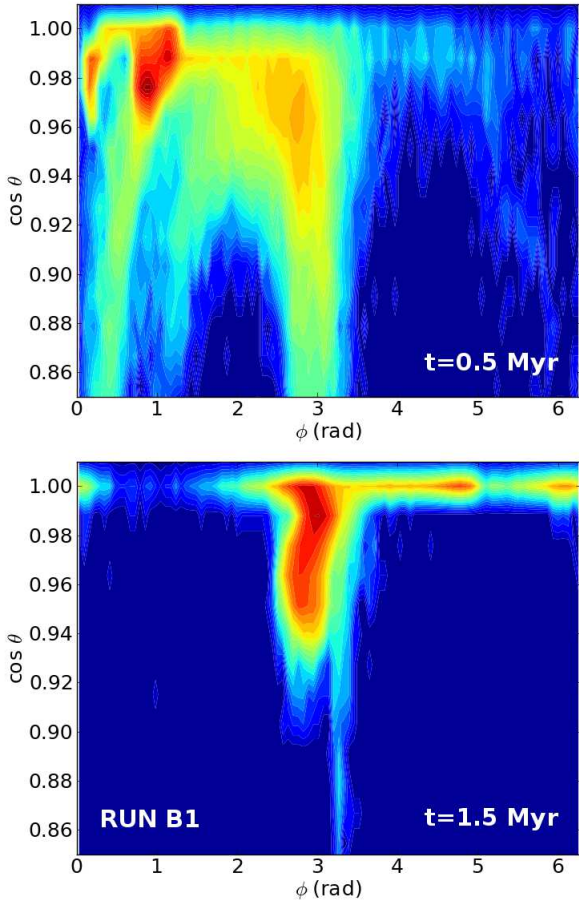


Figure 6. Density of angular momentum vectors of gas in run B1, in the plane defined by $\cos\theta$ and ϕ (see equation A2). Top panel: $t = 0.5$ Myr. Bottom panel: $t = 1.5$ Myr. Only gas particles on bound orbits around the SMBH with semi-major axis $0.1 \leq a/\text{pc} \leq 10$ are shown. The reference system is defined by the total angular momentum of the stellar disc at time t , as described in Appendix A. Note that the zero point of ϕ and θ is not exactly the same between the two panels. The colour map is logarithmic.

inclination between the stellar disc and a second misaligned disc is given by the difference in θ .

From Figs. 6 and 7 it is apparent that the gas discs are neither razor-thin nor regular structures. In particular, the top panels of Figs. 6 and 7 show that the situation is rather complicated at $t = 0.5$ Myr, i.e. during the first phase of the disc assembly (see also Figs. 4 and 5). At $t = 1.5$ Myr the gas discs are more coherent, especially in the case of run B2 (bottom panel of Fig.7), where the angular momentum vectors concentrate at $\cos\theta = 0.964$ and $\phi = 3$ rad. In both runs B1 and B2, the total angular momentum direction of the main gas disc is similar to the one of the stellar disc, but is slightly offset. The offset at $t = 1.5$ Myr is $\sim 10^\circ$ and $\sim 15^\circ$ in runs B1 and B2, respectively. These issues are very important for the effects of the gas on the stellar orbits, as it will be discussed in Section 3.3.

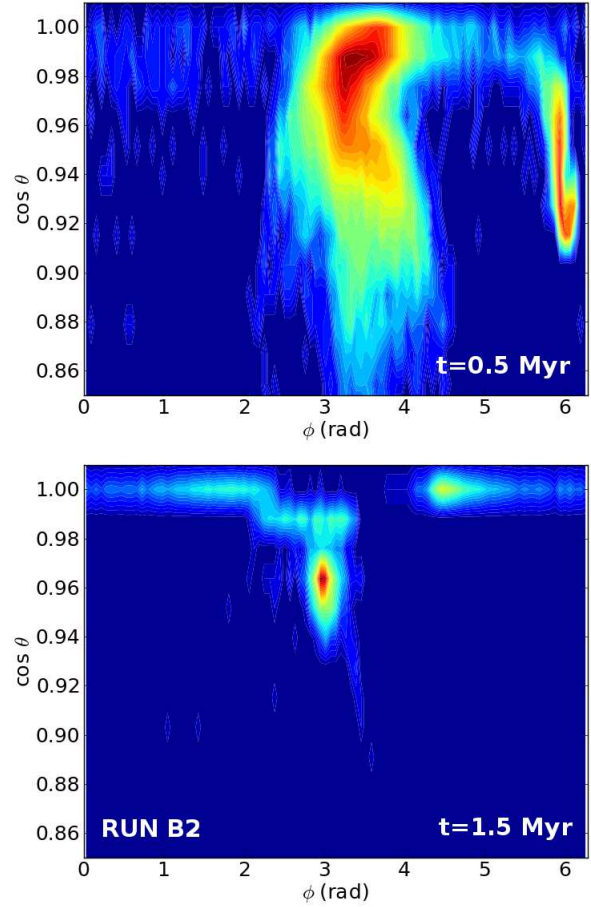


Figure 7. The same as Fig. 6, but for run B2.

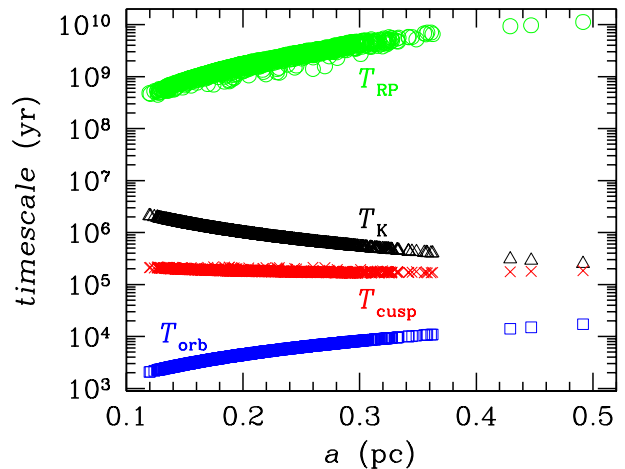


Figure 8. Comparison of the relevant timescales as a function of the semi-major axis for run B2. Open circles: T_{RP} ; open triangles: T_{K} ; crosses: T_{cusp} ; open squares: T_{orb} .

3.2 Timescales for precession

The two main sources of perturbation of the stellar orbital inclinations in our simulations are: (i) the precession induced by the rigid stellar cusp; (ii) the precession induced by the disrupted molecular cloud. In this section, we give an estimate of the timescales associated with these precessions, for the quantities involved in our simulations.

(i) The stellar cusp, i.e. a spherical potential, induces a precession of the orbits of the disc stars on a timescale (Ivanov et al. 2005; Löckmann & Baumgardt 2008; Löckmann et al. 2009; G12)

$$T_{\text{cusp}} = \frac{M_{\text{SMBH}}}{M_{\text{cusp}}} T_{\text{orb}} f(e), \quad (1)$$

where M_{SMBH} is the mass of the SMBH, T_{orb} is the orbital period of a disc star, M_{cusp} is the mass of the cusp inside the stellar orbit, and $f(e) = \frac{1+\sqrt{1-e^2}}{\sqrt{1-e^2}}$ is a function of the eccentricity e of a disc star. The main effect of this precession is pericentre advance (e.g. Šubr & Haas 2012).

(ii) The disrupted molecular cloud settles into a dense and irregular gas disc. The newly formed gas disc and the pre-existing stellar disc exert mutual torques on each other, and thus precess about each other. A star orbiting a SMBH of mass M_{SMBH} with semi-major axis a , at an inclination β relative to a gas disc of radius R_{DISC} and mass M_{DISC} precesses on a timescale (Nayakshin 2005; Löckmann et al. 2008; Šubr et al. 2009):

$$T_{\text{DISC}} \sim \frac{T_{\text{K}}}{\cos \beta} \frac{\sqrt{1-e^2}}{1 + \frac{3}{2}e^2}, \quad (2)$$

where

$$T_{\text{K}} \equiv \frac{M_{\text{SMBH}}}{M_{\text{DISC}}} \frac{R_{\text{DISC}}^3}{a^{3/2} \sqrt{G M_{\text{SMBH}}}}. \quad (3)$$

T_{DISC} is the timescale for the change of the longitude of the node, i.e. for the precession around the symmetry axis of the gaseous disc (Šubr & Haas 2012). T_{DISC} depends on the inclination between the two discs, and in particular T_{DISC} tends to infinity if $\beta \approx 90^\circ$: the precession will be very slow if the two discs are perpendicular. Instead, T_{DISC} is minimised, or in other words, the precession occurs at its maximal rate, if the two discs are coplanar. Furthermore, the precession timescale depends on the distance of the star from the SMBH ($T_{\text{DISC}} \propto a^{-3/2}$). Thus, stars with different a will precess with different speed.

If $\beta = 0$ and the two discs are razor thin, then the precession does not affect the inclinations, as it is just a change of the longitude of the node. Instead, if $\beta \gtrsim 5^\circ$, this precession significantly influences the inclinations of stellar orbits (Löckmann et al. 2008; Šubr et al. 2009). In the latter case, the orbits of the outer stars will become inclined with respect to the orbits of the inner stars, producing a warp in the disc, and increasing its thickness.

Kozai oscillations are another possible effect induced by the interaction between two discs. They trigger a periodic increase of the eccentricity together with small variations of the inclination, and their characteristic timescale is $\propto T_{\text{K}} \sin^{-2} \beta$ (see Šubr et al. 2009). Kozai oscillations are efficiently damped in presence of a spherical cusp, if $T_{\text{K}} > T_{\text{cusp}}$ (which is the case of our run B2, see Fig. 8). As our integrator is not sufficiently accurate for large eccen-

tricitities, we select a cloud orbit with $\alpha = 0$, so that the final inclination between gas disc and stellar disc remains mild. Thus, Kozai oscillations are negligible³.

Finally, relativistic effects are not included in our code. Thus, we cannot account for the relativistic precession of the orbits due to the SMBH. The timescale for relativistic precession is (see Gualandris & Merritt 2009):

$$T_{\text{RP}} = \frac{2\pi c^2 (1-e^2) a^{5/2}}{3(G M_{\text{SMBH}})^{3/2}}, \quad (4)$$

where c is the speed of light.

Fig. 8 shows a comparison of the relevant timescales for our simulations. It is apparent that the timescale for relativistic precession is $\gtrsim 3$ orders of magnitude longer than the cusp precession timescale. Thus, relativistic precession is negligible for our simulated stellar disc, and the fact that we do not include relativistic effects in our simulations is not an issue. Fig. 8 shows that T_{cusp} is almost independent of the semi-major axis, for the potential well of the stellar cusp in the GC (see G12). On the contrary, T_{K} , which measures the perturbation by the gas disc, depends on the semi-major axis, and is about one order of magnitude shorter for the outermost simulated stars than for the innermost ones. T_{K} is always longer than T_{cusp} . On the other hand, the timescale of disc precession (T_{DISC}) depends on the angle β between the stellar orbit and the gas disc. Furthermore, to derive T_{K} in Fig. 8, we assumed that the disc is regular, that its mass is $4 \times 10^4 M_{\odot}$, and that its radius is 0.5 pc. Each of these assumptions is a source of uncertainty, as the disc is not regular, the radius is not clearly defined and the mass depends on the radius. Finally, Fig. 8 is derived in the case of run B2. The other runs have small differences, which depend on the eccentricity distribution. In the next section, we will consider all the runs in detail.

3.3 The evolution of the stellar disc in the simulations

In this section, we investigate the effect of the perturbations generated by the gas disc on the stellar disc, in our simulations B1 and B2.

In agreement with the fact that the precession cannot affect the semi-major axis of the orbit (from energy conservation, e.g. Šubr et al. 2009), the distribution of semi-major axes is not perturbed by the second cloud (bottom row of Fig. 9). Instead, the distribution of inclinations is significantly affected by the gas disc, in both run B1 and B2 (top row of Fig. 9). In fact, the precession induced by the presence of the gas disc is maximum when β is small (see equation 2), and its effect on inclinations is not suppressed by the presence of the stellar cusp (see e.g. Šubr et al. 2009). Actually, if the gas disc was perfectly razor-thin and coplanar with the stellar disc ($\beta = 0$), we would not have found significant

³ As we discussed in the previous Section, the gas disc is not a rigid body, but a collection of concentric annuli with rather different inclination. On the other hand, we exclude that Kozai oscillations play a role, as we do not see any difference in the eccentricity evolution between run B1 (in which there is no stellar cusp) and run B2 (where Kozai oscillations should be damped by the stellar cusp).

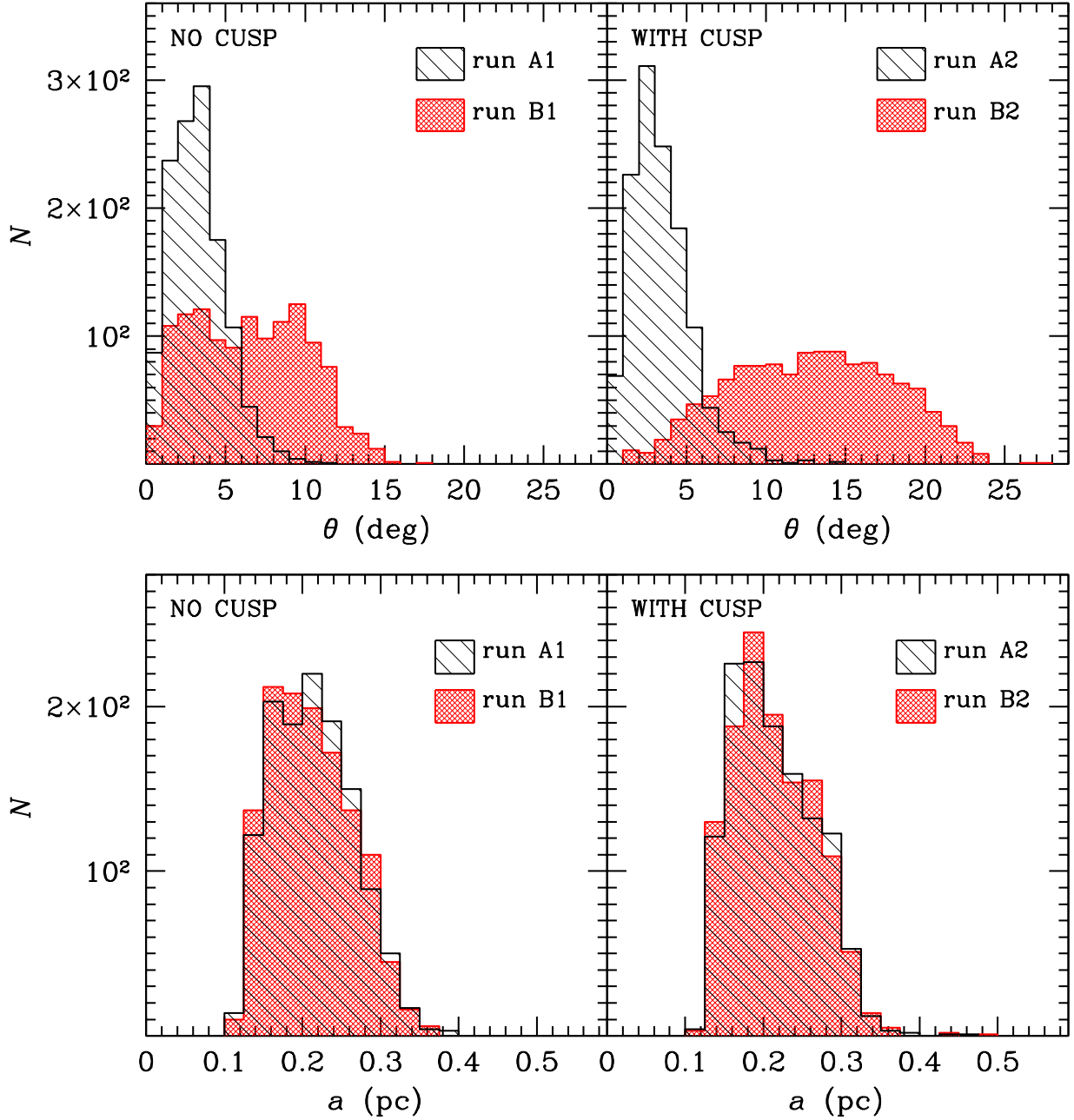


Figure 9. Top (bottom): distribution of inclinations (semi-major axes) at $t = 1.5$ Myr. The inclinations are measured by the angle θ , between the normal vector to the orbit of a single star and the total angular momentum vector of the stellar disc (see Appendix A). Left-hand panel: run B1 (cross-hatched red histogram) and run A1 (hatched black histogram). Right-hand panel: run B2 (cross-hatched red histogram) and run A2 (hatched black histogram).

changes in the inclinations (e.g. Šubr et al. 2009), but just the precession of the ascending node. On the other hand, as we showed in Section 3.1, the simulated gas disc is neither razor thin nor perfectly coplanar with the stellar disc. Values of β as high as $5 - 20^\circ$ occur in some of the streamers, and lead to the increase of the inclinations in a rather complex way.

The fact that stellar inclinations in run B2 are generally larger than those in run B1 can be attributed to the different potential well. In fact, in run B2 the cloud is disrupted marginally faster than in run B1, as the potential well of

run B2 is the combination of the SMBH and of the stellar cusp. For this reason, the stars in run B2 are exposed to the influence of the gas disc for a longer time than the stars in run B1. Also, stochastic fluctuations leading to slightly different inclinations of the streamers might play an important role.

Table 2 summarizes some of the main statistical properties of the simulations. In run B1 (B2), the average inclination passes from 2.4° (2.4°) at $t = 0$ to 6.6° (12.9°) at $t = 1.5$ Myr since the beginning of the simulation (corresponding to $t = 1.98$ Myr since the beginning of run E in

Table 2. Main statistical properties of the simulations at $t = 1.5$ Myr.

Run	$\langle a \rangle$ (pc)	$\langle e \rangle$	$\langle \theta \rangle$ ($^\circ$)	a_{\max} (pc)	e_{\max}	θ_{\max} ($^\circ$)
A1	0.21 ± 0.05	0.3 ± 0.1	3.3 ± 1.7	0.40	0.6	11.9
A2	0.21 ± 0.05	0.3 ± 0.1	3.4 ± 1.9	0.47	0.7	14.4
B1	0.21 ± 0.05	0.3 ± 0.1	6.6 ± 3.5	0.37	0.6	17.3
B2	0.21 ± 0.05	0.3 ± 0.1	12.9 ± 5.0	0.49	0.8	27.2
G12	0.21 ± 0.05	0.3 ± 0.2	3.5 ± 2.1	0.49	0.7	13.8

Average semi-major axis ($\langle a \rangle$), average eccentricity ($\langle e \rangle$), average inclination ($\langle \theta \rangle$), maximum semi-major axis (a_{\max}), maximum eccentricity (e_{\max}) and maximum inclination (θ_{\max}) in our simulations, at $t = 1.5$ Myr. The provided uncertainty on the average values is the standard deviation. In the last row, we report the simulation presented by G12, for comparison with our run A2. The initial values are the same for all the simulations (by construction), and are $\langle a \rangle = 0.21 \pm 0.04$ pc, $\langle e \rangle = 0.29 \pm 0.04$, $\langle \theta \rangle = 2.4 \pm 1.5^\circ$, $a_{\max} = 0.39$ pc, $e_{\max} = 0.44$ and $\theta_{\max} = 7.5^\circ$.

M12). The maximum achieved inclination is 17.3° and 27.2° in run B1 and B2, respectively.

We find no statistically significant differences for the average semi-major axes and for the average eccentricities. We also checked whether or not the orbital properties of the simulated stars depend on the stellar mass, and we found no statistically significant difference (at more than 1σ) between stars with mass $> 5 M_\odot$ and stars with mass $< 5 M_\odot$.

In Fig. 10, the inclinations are shown as a function of the semi-major axis for run A2 (without gas disc) and run B2 (with gas disc), at $t = 1.5$ Myr. For comparison, we report the initial conditions. In Fig. 10, the inclinations of the individual stellar orbits were re-binned in four different bins (so that each bin contains at least 25 stars). In the initial conditions, the average inclinations in each bin are well below 7° . The inner stellar orbits appear more inclined than the outer ones, because the gas disc in run E of M12 formed with this feature (see M12 for details). In run B2, the average inclinations ($> 10^\circ$) are significantly higher than those in the initial conditions, and it is apparent that the outer stellar orbits achieve (on average) higher inclinations than the inner ones. This is an effect of the precession induced by the gas disc: as $T_K \propto a^{-3/2}$, the outer orbits are expected to precess faster than the inner ones. As a further support that this is a genuine effect of precession, induced by the gas disc, the inclinations in run A2 (without gas) remain almost the same as they are in the initial conditions. Furthermore, Fig. 10 indicates that the half-opening angle of the stellar disc at $t = 1.5$ Myr is as large as $\sim 15^\circ$ in run B2, while it does not exceed $\sim 7^\circ$ in run A2. Because of this semi-major axis dependent change in the inclinations, the simulated stellar disc in run B2 (and, similarly, in run B1) may appear tilted and/or warped.

Recent observations (Bartko et al. 2009, 2010; Lu et al. 2009; Do et al. 2013; Lu et al. 2013) show that the opening angle of the CW disc is only $\sim 10^\circ - 14^\circ$, but about half of the early-type stars in the inner $1 - 10$ arcsec ($0.04 - 0.4$ pc) do not belong to the CW disc. Furthermore, the probability of early-type stars being members of the CW disc

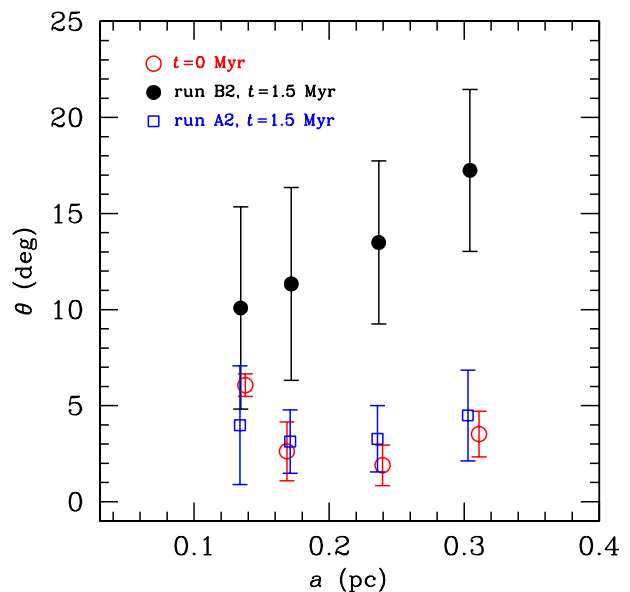


Figure 10. Inclination (with respect to the direction of the average angular momentum) as a function of the semi-major axis in the initial conditions (open red circles), in run A2 at $t = 1.5$ Myr (open blue squares) and in run B2 at $t = 1.5$ Myr (filled black circles). The inclinations of the individual stellar orbits were rebinned in four different bins (each bin was chosen to contain at least 25 stars). Each point is the average inclination per bin, while the error bars show the standard deviation for each bin.

decreases with increasing projected distance from Sgr A* (Bartko et al. 2009; Lu et al. 2009). Finally, the CW disc does not seem a flat structure, but rather a significantly warped ($\sim 64^\circ$, Bartko et al. 2009) and tilted object.

Our simulations suggest a reasonable interpretation for such observations: the precession exerted by a slightly misaligned gas disc enhances the inclinations of the outer stellar orbits with respect to the inner stellar orbits. Thus, while the inner disc remains quite coherent, the outer stellar orbits change angular momentum orientation till they may even lose memory of their initial belonging to the same disc. The result is a tilted/warped disc, which is being dismembered in its outer parts. By the time our simulations were stopped (1.5 Myr), the warping is still lower than the observed effect. On the other hand, it is reasonable to expect that in few Myr the simulated disc will match the observed features.

A similar interpretation was already proposed by Šubr et al. (2009; see also Haas et al. 2011a, 2011b), which pointed out the possible influence of the CNR on the stellar disc. Our paper supports the results by Šubr et al. (2009), by means of the first self-consistent N-body/SPH simulations. Other studies considered similar effects induced by a second stellar disc (Löckmann et al. 2009, 2009b). Alternatively, radiation pressure instability or the Bardeen-Petterson effect were also invoked as possible sources of warping, both driven by the central SMBH (Ulubay-Siddiki et al. 2013). It is likely that the complex distribution of early-type stars

in the GC is due to the concurrence of different proposed mechanisms.

3.4 One or two gas discs?

One of the most simplistic assumptions of our simulations is that no gas is left in the initial disc, as we instantaneously removed the remaining gas disc in run E of M12. This is necessary to prevent our simulations from stalling before the infall of the second cloud. On the other hand, we do not know whether the feedback from the SMBH and/or from the newly born stars is sufficiently efficient to remove all the gas in ≈ 0.5 Myr (e.g. Alexander et al. 2012). For a typical young star cluster with mass $\sim 5 \times 10^3 M_{\odot}$ and radius ~ 0.5 pc, gas expulsion is expected to occur in $\sim 10^5$ yr, because of the photo-ionizing flux from O stars (Kroupa & Boily 2002). However, the case of the young stellar disc in the GC is more tricky, as the disc is dominated by the gravitational field of the SMBH⁴ and of the stellar cusp. Furthermore, the gas in the disc has a density of $\sim 10^{7-8} \text{ cm}^{-3}$, implying that the Strömngren sphere around a O star is only $\sim 10^{-3}$ pc. Dynamical effects (e.g. Mathews & O’dell 1969; Franco et al. 1990) might increase the radius of the ionized region around early-type stars, but it is more likely that the gas disc can be completely evaporated only by the first supernovae in the stellar disc ($\gtrsim 3$ Myr). Finally, a possible contribution from the SMBH or other ionizing sources in the GC is even less constrained.

In summary, our assumption of instantaneous removal of the gas from the first disc, although necessary to avoid serious computational-time issues, might underestimate the gas evaporation timescale. This does not alter the dynamical evolution dramatically, as the gravitational influence of the SMBH on the stellar disc is larger by more than two orders of magnitude with respect to that of the gas disc. However, the first gas disc, if not completely removed, is expected to contribute to the secular evolution of the stellar disc. This effect is not included in our simulations.

On the other hand, our simulations provide important information, even if the actual evaporation timescale is longer. In this case, our simulations can be considered as a robust lower limit to the effect of a second gas disc. In fact, if the first gas disc was not completely evaporated by the time the second gas disc forms, the effects of the latter may combine with those of the former, and the resulting precession induced on the stellar disc is expected to be even stronger.

In the extreme case of almost no gas evaporation in 2 Myr, the results of our simulations mimic the secular influence exerted on the stellar disc by its parent gas disc, rather than the perturbations induced by a second gas disc. This implies that even a long-lived (> 1 Myr) parent gas disc can significantly affect the inclinations of the stellar orbits.

⁴ The radiation pressure exerted by a star on a hydrogen atom overcomes the gravitational pull by the SMBH only when the distance of the hydrogen atom from the star is $d_* \leq 10^{-3} (L_*/10^{39} \text{ erg s}^{-1})^{1/2} (M_{\text{SMBH}}/3.5 \times 10^6 M_{\odot})^{-1/2} d_{\text{BH}}$, where L_* is the luminosity of the star and d_{BH} is the distance of the hydrogen atom from the SMBH.

4 CONCLUSIONS

In this paper, we study the effect of perturbations caused by a molecular cloud spiralling towards the GC on the orbits of a pre-existing stellar disc. It is likely that fresh gas spiralled to the GC in the last few Myrs, as Yusef-Zadeh et al. (2013) observe the traces of very recent star formation (10^{4-5} yr) in the inner parsec.

In our N-body/SPH simulations, the pre-existing stellar disc was formed by a first molecular cloud, disrupted by the GC (run E of M12). We simulate a second molecular cloud that falls towards the GC, is disrupted by the SMBH, and settles into a dense gas disc. The gas disc perturbs the orbits of the stellar disc. The details of this perturbation depend on the orbital parameters of the two discs and on the presence of a stellar cusp. The gas disc is neither razor-thin nor regular: it is a collection of different streamers with slightly different inclinations. The inclination of the angular momentum vector of the single streamers with respect to the angular momentum vector of the stellar disc ranges from ~ 0 to $\sim 20^\circ$. Thus, the dynamical interplay between the stellar disc and the gaseous disc(s) is highly complex.

Our simulations show that, if the gas disc and the stellar disc are slightly misaligned ($\sim 5 - 20^\circ$), the precession induced by the gas disc leads to a significant increase of the inclinations of the stellar orbits. The inclinations of the outer stellar orbits increase more than those of the inner ones, as the precession is faster for larger semi-major axes. This has crucial implications for the evolution of a stellar disc in the GC.

In fact, the probability of early-type stars being members of the CW disc decreases with increasing projected distance from Sgr A* (Bartko et al. 2009; Lu et al. 2009). Furthermore, the CW disc does not seem a flat structure, but rather a significantly warped ($\sim 64^\circ$, Bartko et al. 2009) and tilted object.

Our simulations suggest that the outer stellar orbits lose coherence with their original disc because of differential precession. This has two main effects: (i) the stellar disc appears warped/tilted; (ii) the outer parts of the stellar disc are progressively dismembered. This is consistent with previous predictions by Šubr et al. (2009), which proposed that the CNR is the source of differential precession.

In our simulations, we assumed that the parent gas disc instantaneously evaporated, and that the naked stellar disc interacts with a second molecular cloud. It is likely that the stellar disc is still embedded in some residual of the original gas disc. Thus, our simulations provide a robust lower limit to the effect of a second gas disc. In fact, if the first gas disc was not completely evaporated, the new disc ‘superimposes’ to the old one, and the resulting precession induced on the stellar disc is expected to be even stronger.

Another effect expected to be important is Kozai resonance. In our simulations, Kozai resonance is negligible as the timescale for Kozai oscillations scales as $\propto T_K \sin^{-2} \beta$. Kozai resonance becomes important only if $\beta \gg 0$, but might be completely suppressed by the stellar cusp (e.g. Šubr et al. 2009). The case with $\beta \sim 90^\circ$ deserves to be investigated with a more suitable integration scheme. Finally, we do not observe fragmentation in the simulations presented in this paper, but the mass resolution of gas particles is a factor of 10 lower than in M12. Thus, the pos-

sibility that the second gas disc fragments into self-bound clumps, forming stars, will be addressed in a further study, with higher resolution simulations.

ACKNOWLEDGMENTS

We thank the referee, Ladislav Šubr, for his valuable comments that significantly improved our paper. We also thank H. Perets, E. Ripamonti, L. Mayer, R. Alexander, W. Dehnen, A. King and S. Nayakshin for useful discussions. We thank the authors of GASOLINE (especially J. Wadsley, T. Quinn and J. Stadel). We acknowledge the CINECA Award N. HP10CL51UF, 2012 for the availability of high performance computing resources and support. MM acknowledges financial support from the Italian Ministry of Education, University and Research (MIUR) through grant FIRB 2012 (‘New perspectives on the violent Universe: unveiling the physics of compact objects with joint observations of gravitational waves and electromagnetic radiation’), and from INAF through grant PRIN-2011-1 (‘Challenging Ultraluminous X-ray sources: chasing their black holes and formation pathways’).

REFERENCES

Agertz O., et al., 2007, MNRAS, 380, 963
 Alexander R. D., Armitage P. J., Cuadra J., Begelman M. C., 2008, ApJ, 674, 927
 Alexander R. D., Smedley S. L., Nayakshin S., King A. R., 2012, MNRAS, 419, 1970
 Alig C., Burkert A., Johansson P. H., Schartmann M., 2011, MNRAS, 412, 469
 Alig C., Schartmann M., Burkert A., Dolag K., 2013, ApJ, 771, 119
 Bartko H. et al. 2009, ApJ, 697, 1741
 Bartko H. et al. 2010, ApJ, 708, 834
 Boley A. C., 2009, ApJ, 695, L53
 Boley A. C., Hayfield T., Mayer L., Durisen R. H., 2010, Icarus, 207, 509
 Bonnell I. A., Rice W. K. M., 2008, Science, 321, 1060
 Christopher M. H., Scoville N. Z., Stolovy S. R., Yun M. S., 2005, ApJ, 622, 346
 Collin S., Zahn J.-P., 2008, A&A, 477, 419
 D’Alessio P., Calvet N., Hartmann L., 2001, ApJ, 553, 321
 Dehnen W., Read J. I., 2011, The European Physical Journal Plus, 126, 55
 Do T., Lu J. R., Ghez A. M., Morris M. R., Yelda S., Martinez G. D., Wright S. A., Matthews K., 2013, ApJ, 764, 154
 Eisenhauer F. et al., 2005, ApJ, 628, 246
 Franco J., Tenorio-Tagle G., Bodenheimer P., 1990, ApJ, 349, 126
 Genzel R., Crawford M. K., Townes C. H., Watson D. M., 1985, ApJ, 297, 766
 Genzel R., et al., 2003, ApJ, 594, 812
 Ghez A. M., et al., 2003, ApJ, 586, L127
 Ghez A. M., et al., 2005, ApJ, 635, 1087
 Gillessen S., Eisenhauer F., Trippe S., Alexander T., Genzel R., Martins F., Ott T., 2009, ApJ, 692, 1075
 Goodman J., 2003, MNRAS, 339, 937

Goodman J., Tan J. C., 2004, ApJ, 608, 108
 Gualandris A., Merritt D., 2009, ApJ, 705, 361
 Gualandris A., Gillessen S., Merritt D., 2010, MNRAS, 409, 1146
 Gualandris A., Mapelli M., Perets H. B., 2012, MNRAS, 427, 1793 (G12)
 Güsten R., Genzel R., Wright M. C. H., Jaffe D. T., Stutzki J., Harris A. I., 1987, ApJ, 318, 124
 Haas J., Šubr L., Kroupa P., 2011a, MNRAS, 412, 1905
 Haas J., Šubr L., Vokrouhliký D., 2011b, MNRAS, 416, 1023
 Harfst S., Gualandris A., Merritt D., Spurzem R., Portegies Zwart S., Berczik P., 2007, NewAstronomy, 12, 357
 Hayfield T., Mayer L., Wadsley J., Boley A. C., 2011, MNRAS, 417, 1839
 Hobbs A., Nayakshin S., 2009, MNRAS, 394, 191
 Ivanov P. B., Polnarev A. G., Saha P., 2005, MNRAS, 358, 1361
 Jiang Y.-F., Goodman J., 2011, ApJ, 730, 45
 Kozai Y., 1962, AJ, 67, 591
 Krabbe A., Genzel R., Drapatz S., Rotaciuc V., 1991, ApJ, 382, L19
 Krabbe A., et al., 1995, ApJ, 447, L95
 Kroupa P., Boily C. M., 2002, MNRAS, 336, 1188
 Larson R. B., 1981, MNRAS, 194, 809
 Levin Y., Beloborodov A. M., 2003, ApJ, 590L, 33
 Lidov M. L., 1962, Planetary and Space Science, 9, 719
 Löckmann U., Baumgardt H., 2008, MNRAS, 384, 323
 Löckmann U., Baumgardt H., Kroupa P., 2008, ApJ, 683, L151
 Löckmann U., Baumgardt H., 2009, MNRAS, 394, 1841
 Löckmann U., Baumgardt H., Kroupa P., 2009, MNRAS, 398, 429
 Lu J. R., Ghez A. M., Hornstein S. D., Morris M., Matthews K., Thompson D. J., Becklin E. E., 2006, JPhCS, 54, 279
 Lu J. R., Ghez A. M., Hornstein S. D., Morris M. R., Becklin E. E., Matthews K., 2009, ApJ, 690, 1463
 Lu J. R., Do T., Ghez A. M., Morris M. R., Yelda S., Matthews K., 2013, ApJ, 764, 155
 Lucas W. E., Bonnell I. A., Davies M. B., Rice K., 2013, MNRAS, 433, 353
 Madigan A.-M., Levin Y., Hopman C., 2009, ApJ, 697, L44
 Mapelli M., Hayfield T., Mayer L., Wadsley J., 2008, arXiv0805.0185
 Mapelli M., Hayfield T., Mayer L., Wadsley J., 2012, ApJ, 749, 168 (M12)
 Mathews W. G., O’dell C. R., 1969, Annual Review of Astronomy and Astrophysics, 7, 67
 Milosavljevic M., Loeb A., 2004, ApJ, 604L, 45
 Morris M., 1993, ApJ, 408, 496
 Namekata D., Habe A., 2011, ApJ, 731, 57
 Nayakshin S., 2005, MNRAS, 359, 545
 Nayakshin S., Cuadra J. J., 2005, A&A, 437, 437
 Novak G., Dotson J. L., Dowell C. D., Hildebrand R. H., Renbarger T., Schleuning D. A., 2000, ApJ, 529, 241
 Oka T., Nagai M., Kamegai K., Tanaka K., 2011, ApJ, 732, 120
 Paumard T. et al., 2006, ApJ, 643, 1011
 Perets H. B., Gualandris A., 2010, ApJ, 719, 220
 Read J. I., Hayfield T., Agertz O., 2010, MNRAS, 405, 1513

- Rice W. K. M., Lodato G., Armitage P. J., 2005, MNRAS, 364, L56
- Schödel R., Ott T., Genzel R., Eckart A., Mouawad N., Alexander T., 2003, ApJ, 596, 1015
- Schödel et al., 2007, A&A, 469, 125
- Solomon P. M., Scoville N. Z., Penzias A. A., Wilson R. W., Jefferts K. B., 1972, ApJ, 178, 125
- Šubr L., Schovancová J., Kroupa P., 2009, A&A, 496, 695
- Šubr L., Haas J., 2012, Journal of Physics: Conference Series, 372, 012018
- Ulubay-Siddiki A., Bartko H., Gerhard O., 2013, MNRAS, 428, 1986
- Wadsley J. W., Stadel J., Quinn T., 2004, NewAstronomy, 9, 137
- Wardle M., Yusef-Zadeh F., 2008, ApJ, 683L, 37
- Yelda S., Ghez A. M., Lu J. R., Do T., Meyer L., Morris M. R., 2012, Adaptive Optics Systems III. Proceedings of the SPIE, Volume 8447, article id. 84470A
- Yusef-Zadeh F., Hewitt J. W., Cotton W., 2004, ApJS, 155, 421
- Yusef-Zadeh F., Braatz J., Wardle M., Roberts D., 2008, ApJ, 683, L147
- Yusef-Zadeh F., et al., 2013, ApJ, 767, L32
- Zemp M., Stadel J., Moore B., Carollo C. M., 2007, MNRAS, 376, 273
- Zhao J.-H., Morris M. R., Goss W. M., An T., 2009, ApJ, 699, 186

APPENDIX A: THE COORDINATE SYSTEM

The coordinate system is defined in the following way. We define \mathbf{J}_{DISC} as the total angular momentum of the stellar disc. The normal vector to the total angular momentum of the stellar disc will then be

$$\mathbf{n}_{\text{DISC}} = \mathbf{J}_{\text{DISC}}/J_{\text{DISC}} = (\cos \phi_{\text{DISC}} \sin \theta_{\text{DISC}}, \sin \phi_{\text{DISC}} \sin \theta_{\text{DISC}}, \cos \theta_{\text{DISC}}), \quad (\text{A1})$$

where J_{DISC} is the modulus of \mathbf{J}_{DISC} . We now define the coordinate system so that $\cos \theta_{\text{DISC}} = 1$ at any given time t . The normal vector to the angular momentum of a single star will then be

$$\mathbf{n} = \mathbf{J}/J = (\cos \phi \sin \theta, \sin \phi \sin \theta, \cos \theta), \quad (\text{A2})$$

where \mathbf{J} and J are the angular momentum vector of a single star orbit and its modulus, respectively. By construction, $\theta = \theta_{\text{DISC}} = 0$ means that the angular momentum of a star is aligned to the total angular momentum of the disc. Thus, we refer to the value of θ as the inclination of the stellar orbit with respect to the disc axis at a given time t . The average value of θ ($\langle \theta \rangle$) gives also a measure of the half-opening angle of the disc. Fig. A1 shows how the stellar orbits populate the plane defined by $\cos \theta$ and ϕ in the initial conditions and in runs A1 and B1. Fig. A2 is the same as Fig. A1, but for runs A2 and B2.

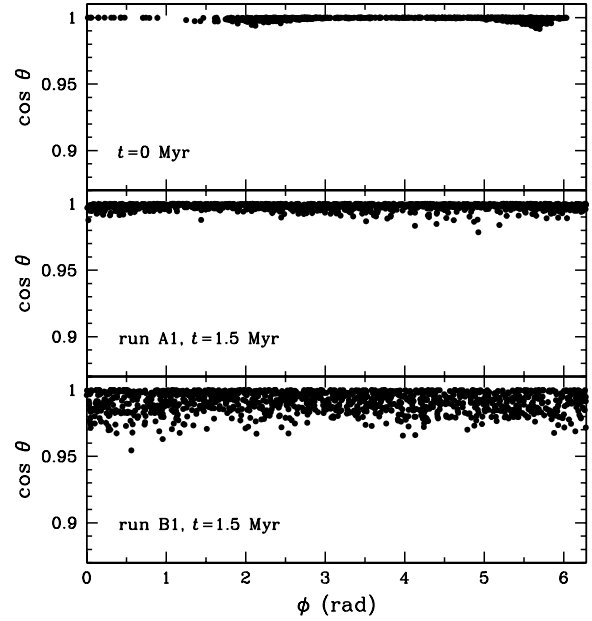


Figure A1. Each point marks the position of a stellar orbit in the plane defined by $\cos \theta$ and ϕ (see equation A2). Top panel: initial conditions (the same for all runs). Central panel: run A1 at $t = 1.5$ Myr. Bottom panel: run B1 at $t = 1.5$ Myr.

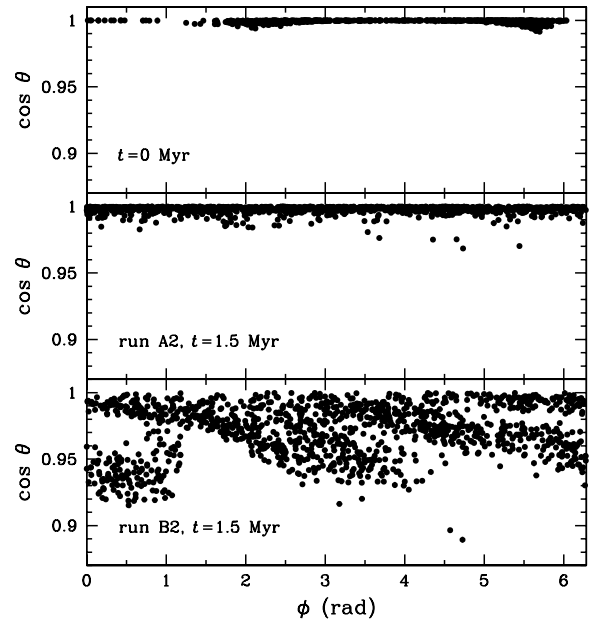


Figure A2. Each point marks the position of a stellar orbit in the plane defined by $\cos \theta$ and ϕ (see equation A2). Top panel: initial conditions (the same for all runs). Central panel: run A2 at $t = 1.5$ Myr. Bottom panel: run B2 at $t = 1.5$ Myr.